Modulation of Vesicle Adhesion and Spreading Kinetics by Hyaluronan Cushions

Laurent Limozin* and Kheya Sengupta†
*Adhésion Cellulaire, Centre National de la Recherche Scientifique UMR 6212, INSERM U600, Université de la Mediterranée, Luminy, Marseille, France; and †Institut für Bio- und Nanosysteme-4 (Biomechanics), Forschungszentrum, Jülich, Germany

ABSTRACT The adhesion of giant unilamellar phospholipid vesicles to planar substrates coated with extracellular matrix mimetic cushions of hyaluronan is studied using quantitative reflection interference contrast microscopy. The absolute height of the vesicle membrane at the vicinity of the substrate is measured by considering, for the first time, the refractive indices of the reflecting media. The thickness of the cushion is varied in the range of ~50–100 nm, by designing various coupling strategies. On bare protein-coated substrates, the vesicles spread fast (0.5 s) and form a uniform adhesion disk, with the average membrane height ~4 nm. On thick hyaluronan cushions (>80 nm), the membrane height is approximately the same as the thickness of the cushion, implying that the vesicle lies on top of the cushion. On a thin and inhomogeneous hyaluronan cushion, the adhesion is modified but not prevented. The spreading is slow (~20 s) compared to the no-cushion case. The average membrane height is ~10 nm and the adhesion disk is studded with blisterlike structures. Observations with fluorescent hyaluronan indicate that the polymer is compressed under, rather than expelled from, the adhesion disk. The adhesion energy density is approximately threefold higher in the no-cushion case (1.2 $\mu J/m^2$) as compared to the thin-cushion case (0.54 $\mu J/m^2$). In the thin-cushion case, the presence of short (~4 nm) glyco-polymers on the vesicles results in a hitherto unreported stable partial adhesion state—the membrane height ranges from zero to ~250 nm. The minimal model system presented here mimics in vitro the hyaluronan-modulated early stages of cell adhesion, and demonstrates that the presence of a polymer cushion influences both the final equilibrium adhesion-state and the spreading kinetics.

INTRODUCTION

The full development of cell adhesion is a complex multistep process that takes up to several minutes, but starts with a first recognition step that occurs over a subsecond timescale (1). A well-known example of such rapid first recognition is the arrest of leukocytes in blood vessels initiated by the fast interaction of selectin molecules with the ligands on the endothelial cells (2). Active cellular response is unlikely to occur over such short timescales and therefore, passive interactions of physical origin are expected to play an important role in the initial steps of adhesion (3), pointing to the need of physical approaches to study these processes.

Recently, the cell surface polysaccharide hyaluronan has been proposed as a possible candidate for mediating the first recognition in certain cell types (4). Hyaluronan (also known as hyaluronic acid, HA) is a linear polyelectrolyte, negatively charged at neutral pH. In water, it assumes an expanded structure, occupying a very large domain, leading to entanglement and viscoelastic behavior at relatively low concentrations (~0.1 mg/ml). Dramatic changes in the amount and organization of extracellular HA occurs during periods of intense cell division activity; for example, during embryogenesis and wound healing as well as malignant tumorigenesis (5). The presence of excess hyaluronan at the cell surface is known to hinder adhesion of cells (6). The ability of thick HA cushions to prevent adhesion of populations of cells have been studied in the context of biomedical applications (7). HA receptors and associated hyaluronan are found on the surface of virtually every animal cell: in some cells like chondrocytes, HA forms a thick, hydrated, pericellular coat (8). Cell surface HA-receptors like CD44 span the cell membrane and connect to HA on one hand, and via other linking proteins, to intracellular actin on the other hand. Furthermore, studies indicate that HA can also initiate intracellular signaling via cell surface receptors (6). Conversely, passive interactions are putatively responsible for the dual repulsive-adhesive role (6,8) ascribed to cell surface hyaluronan, which has been recently probed in great detail (4). It has emerged that even though an excess of hyaluronic acid present in-between the cell surface and an adhesive wall prevents cell adhesion, moderate amounts of the same polymer promotes a weak adhesion state that precedes integrin-mediated adhesion (1,4), presumably by spanning the two interacting surfaces which themselves remain ~1 μm apart (for chondrocytes). Because of the important biological role of HA cushions, in vitro models of surface-coupled hyaluronan of various degrees of biomimicry have been designed and characterized (9–12), with the ultimate aim of understanding the interaction of cells with such layers. In this context, a crucial question is to understand the origin of the reorganization of the surface hyaluronan during the adhesion process.

The short timescale events that initiate cell adhesion are the subject of intense recent research (1,13). A biophysical

Submitted January 30, 2007, and accepted for publication May 29, 2007.

Address reprint requests to K. Sengupta, E-mail: k.sengupta@fz-juelich.de.
K. Sengupta's current address is CRMC-N (UPR CNRS 7251), Luminy, Marseille, France.

Editor: Petra Schwille.

0006-3495/07/11/3300/14 $2.00
doi: 10.1529/biophysj.107.105544

approach toward understanding these early events in cell adhesion is the study of interaction of cell-mimetic giant unilamellar vesicles (GUVs, whose walls mimic the cell membrane) with a suitably modified surface. These vesicles have been extensively used to probe, in addition to adhesion (14–18), various aspects of cell-membrane mechanics (19), and organization (20). This mimetic modeling approach is particularly suitable for study of early stages of cell-surface contact, for example via HA, where passive rather than active processes dominate (1). However, most reported experiments deal with equilibrium situations whereas data on adhesion dynamics remains sparse and contradictory (16–18).

In the case of cells, the main attractive force arises from specific interactions between cell surface proteins. In addition, unspecific interactions of physical origin (e.g., electrostatic, hydrophobic, and van der Waals) also play a significant role in adhesion (3,21). Moreover, cell surface polymers (the glycocalyx (18) in general, and the hyaluronan pericellular coat (1,4) in particular) give rise to a repulsive force of entropic origin (21). The glycocalyx has been mimicked, in GUVs, by including lipids whose headgroups exhibit a short (~4 nm diameter of gyration) polymer chain that diffuse freely in the vesicle membrane (15,18). The inclusion of such polymers has been shown to suppress unspecific adhesion (22) and to slow down the adhesion kinetics (18). Considering that the cell may regulate the mobility of the polymers of the glycocalyx (23), it is important to test the behavior of cells or cell models on immobile polymer cushions.

Reflection interference contrast microscopy (24–26) has proven to be a powerful tool for vesicle adhesion studies and has revealed a variety of interesting phenomena of physical origin that underlie membrane-substrate interaction (14–18,22). Reflection interference contrast microscopy (RICM) has also been used to study cell adhesion (27) but quantitative interpretation of data in this context is more difficult because of possible multiple reflection from organelles and the influence of intracellular refractive index. For these reasons, RICM has not been as broadly used in case of cell as in case of vesicle adhesion. In context of vesicles, the RICM analysis usually considers reflection from only two interfaces, and treats the vesicle membrane as infinitely thin. This treatment is adequate for measuring the contact angle and spreading times but is not sufficient for even a qualitative description of the adhesion zone in terms of the local membrane-substrate distance.

In this article, we present experiments aimed at mimicking, in vitro, the interaction of the cell membrane with a substrate in presence of an intervening hyaluronan rich pericellular coat. HA cushions of different thickness and homogeneity are produced by charge-induced absorption to glass covered either with poly-L-lysin (two different molecular weight) or with avidin. Cell mimetic giant phospholipids vesicles, monitored by RICM, are allowed to interact with the protein-coated surfaces in the presence or absence of the HA cushion. We establish an improved analysis of RICM images which accounts for reflection from the outer-buffer/membrane as well as inner-buffer/membrane interfaces and yields absolute membrane-substrate distances in the adhesion zone. The interaction of the vesicles with the substrate, which is dominated by attractive unspecific forces, is found to be strongly dependent on the thickness of the hyaluronan cushion, leading to various adhesion and spreading scenarios.

MATERIALS AND METHODS

Lipids, proteins, polymers, and beads

All lipids, 1,2-dimyristoyl-*sn*-glycero-3-phosphocholine (DMPC), dimyristoylphosphoethanolamine-poly(ethylene glycol) 2000 (DMPE-PEG2000), and dimyristoylphosphoethanolamine-biotin (DMPE-Biotin) are from Avanti Polar Lipids (Alabaster, AL). Avidin, poly-L-lysin bromide salt (PLL; 80 kDa, and 300 kDa), hyaluronate lyase, high-molecular-weight hyaluronic acid (hyaluronan, potassium salt), biotinylated hyaluronan, and fluorescein-labeled hyaluronan are from Sigma-Aldrich (Hannover, Germany). All the chemicals are used as is without further purification. Colloidal beads used for colloidal probe interference microscopy are polystyrene sulfate particles of diameter 9.6 μm (Interfacial Dynamics, Eugene, OR), coated with bovine serum albumin (Sigma).

Vesicles, substrates, and buffers

Giant unilamellar vesicles are prepared by electro-swelling (see, for example, (15) or (19)). The membrane compositions used in this work are

1. 1:1 molar ratio of DMPC and cholesterol (referred to as ''DMPC vesicles'').
2. Same as composition 1, with 1 mol % DMPE-Biotin added (referred to as ''biotin vesicles'').
3. Same as composition 1, with 5% DMPE-PEG2000 added (referred to as ''PEG vesicles'').

Thickness-corrected glass cover slides (Assistant, Karl Hecht, Sondheim, Germany) are cleaned with a detergent (Hellmanex, Helma, Germany) as described elsewhere (11). Coating of the glass surface by PLL or avidin is realized through charge-induced absorption of the protein by incubation in either phosphate-buffered saline (PBS) (for PLL) or 20 mM phosphate buffer with no added monovalent ions (for avidin). A range of 200 μl to 1 ml of 0.01 mg/ml solution of the protein is incubated for ½ h and the unbound protein is washed off. To further coat the surface with hyaluronan, 200 μl to 1 ml of 0.01 mg/ml solution of hyaluronan (1:1 ratio by weight of biotinylated and unmodified) is incubated for ½ h and the unbound hyaluronan is removed by repeated washing. For confocal measurements, the cushions are prepared with bound fluorescently-labeled hyaluronan (fl-HA) mixed with biotinylated hyaluronan (1:1, 10 μg/ml), incubated for 30 min on a cover slide coated with avidin or PLL. The supernatant is washed carefully after incubation.

Unless specifically mentioned, the vesicle swelling buffer consists of sucrose at an osmolarity of 295 mOsM and the external buffer is PBS at 320 mOsM (thus yielding partially deflated vesicles with expected reduced volume of ~0.93). In certain cases (for validation of RICM analysis), either sucrose at 2550 mOsM (outer buffer PBS+KCl) or glucose at 80 mOsM (outer-buffer-diluted PBS) is used. In all cases, the vesicles are partially deflated. The osmolarity of the buffers is measured with an osmometer (Osmomat 030, Gonotec, Germany). The osmolarity of the vesicle solution after swelling and the final osmolarity of the outer medium after the experiment are also measured. Similarly, refractive indices are measured using an Abbe-refractometer (Krüss Optronics, Hamburg, Germany).

Image acquisition and processing

RICM images are acquired with a Zeiss Axiovert 200 inverted microscope (Carl Zeiss, Jena, Germany) equipped with a 63× antiflex objective and either a PCO camera (PCO, Kelheim, Germany), interfaced to a computer via the acquisition software OpenBox (28) or a C7780 camera with the software Wasabi (both Hamamatsu, Tokyo, Japan). White light emitted by a HBO lamp is filtered using a green filter ($\lambda = 546 \pm 12$ nm) (or in some cases, specifically mentioned, with a blue filter (436 ± 20 nm)). For vesicles, typical exposure times range from 20 to 100 ms. For the colloidal probe interference microscopy, time-lapse RICM is used to follow the height of colloidal particles by measuring the radii of Newton rings as a function of time (11,26). One-hundred consecutive images (total duration 10 s, individual exposure time 10 ms) of the interference pattern are recorded for 60 different beads, located at different positions for each substrate. Confocal fluorescence measurements are realized with a Zeiss LSM-510 scanning confocal microscope, with a 1.40 NA 63× objective and blue laser excitation (488 nm), and comparison is made between images obtained in similar conditions of illumination and exposure time. The pinhole is set to impose an optical slice thickness of ~0.4 μm. Wide-field epifluorescence micrographs for Fig. 7 are taken with a Zeiss Axiovert 200 with 1.45 NA 100× objective and an Andor iXon camera (Andor, Belfast, Ireland) with exposure time of 1 s. All analysis is done using the image analysis software Image-J (public domain, National Institutes of Health) and/or the general-purpose mathematical software Igor-Pro (Wavemetrix, Portland, OR), using self-written routines.

Data analysis

Identification of the contact zone and adhesion zone in RICM

For a sedimented vesicle, the planar bottom, which is close to the substrate and exhibits strong fluctuations (indicated by strongly changing intensity in RICM), is called the contact zone. Upon adhesion, the contact zone develops nonfluctuating adhesion zones, where the adhesion is tight and which may span the whole of the contact zone. In RIC micrographs, the adhesion zone typically appears as a disk with more or less uniform intensity, surrounded by fringes.

RICM of vesicles—interference of reflection from three interfaces

Reflection interference contrast microscopy (RICM) is based on the principle of Newton's rings' formation. The vesicle-membrane-to-substrate distance is calculated from the grayscale interference pattern arising from the interference between light rays reflected from the substrate-buffer interface and the membrane-buffer interface. Traditionally, this simple theory has been used to evaluate RICM data from vesicles (14–18,22,26). However, for quantitative analysis, especially when the inner-buffer exhibits a refractive index that is less than that of the vesicle membrane (as is the case here), reflection from three interfaces have to be considered (Fig. 1 *A*). In this case, generalizing from the literature (24,25), the normalized reflectance R_{norm} (which determines the observed intensity for a given incident intensity) depends on the height as

$$R_{\mathrm{norm}} = \left| 1 + \left[(1 - r_{01}^2) e^{4\pi i n_1 \frac{h}{\lambda}} \left(r_{12} + r_{23}(1 - r_{12}^2) e^{4\pi i n_2 \frac{d_{\mathrm{lipid}}}{\lambda}} \right) \right]^2 / r_{01} \right|^2 - 1$$

and

$$r_{01} = \frac{(n_0 - n_1)}{(n_0 + n_1)}; \quad r_{12} = \frac{(n_1 - n_2)}{(n_1 + n_2)}; \quad r_{23} = \frac{(n_2 - n_3)}{(n_2 + n_3)}, \quad (1)$$

where λ is the wavelength of incident light, n_X is the refractive index of X^{th} layer (see Fig. 1 *A*), d_{lipid} is the thickness of the lipid layer taken to be 4 nm (24), and h is the membrane-substrate distance in which we are interested. For a given pair of n_1 and n_3 (refractive index outer buffer and inner buffer, respectively, henceforth referred to as n_{out} and n_{in}), the dependence of the normalized intensity on height is

$$R_{\mathrm{norm}} = y_0 - A\cos\left(4\pi \frac{n_{\mathrm{out}}}{\lambda}(h - h_0)\right), \quad (2)$$

where y_0, A, and h_0 are constants, determined numerically by fitting Eq. 2 to the result of Eq. 1. Alternatively, the analytical expression of A and h_0 is given in the Appendix. It turns out that the period $\lambda/2n_{\mathrm{out}}$ of this sinusoid remains the same as that expected from the traditional analysis. The height h_0 corresponds to the minimum of the intensity and depends on the values of the inner and outer buffer refractive indices. The traditional RICM analysis (15,18) underestimates the height by an amount h_0. Determining the value of h_0 for given inner and outer buffers is an important step in this analysis.

When the refractive index of the inner buffer is sufficiently high, the minimum of the intensity corresponds to a membrane-substrate distance (h) of almost zero; for example, for $n_{\mathrm{out}} = 1.33$, n_{in} should be at least 1.4 for this distance to be ~5 nm. However, when n_{in} decreases, the minimum of the intensity occurs at non-zero h. Fig. 1 *B* depicts, for a given n_{out} (= 1.332), the expected intensities for n_{in} varying from 1.332 (refractive index of PBS) to 1.486 (refractive index of lipids (24)), and membrane-substrate distance (h)

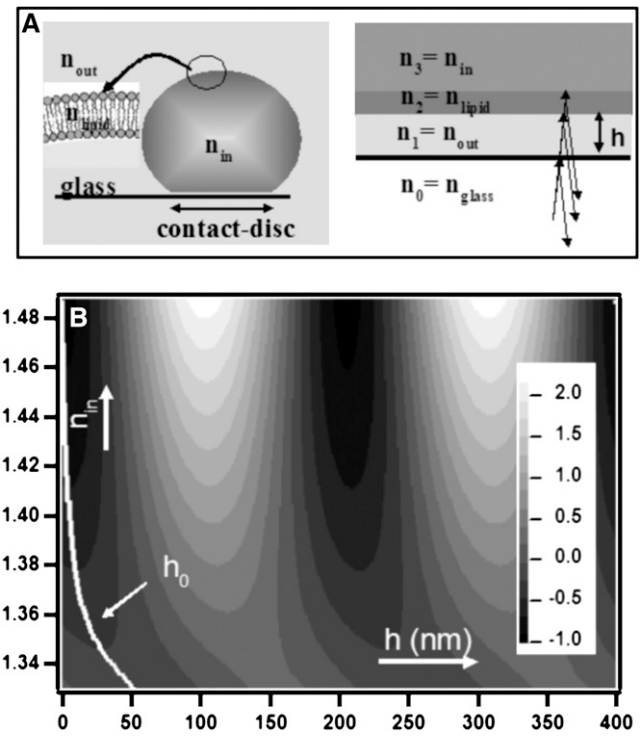

FIGURE 1 (*A*) Schematic representation of a vesicle hovering over a glass slide, with the membrane-substrate distance = h, exhibiting a contact disk (refractive index of inner buffer = n_{in}, of outer buffer = n_{out}, and of the vesicle wall = n_{lipid}); and reflection from the three interfaces that have to be taken into account for quantitative interpretation of RICM of vesicles. (*B*) Expected reflectance (R_{norm}: see Eq. 1, normalized with respect to the expected background), plotted as a function of the refractive index of the inner buffer (n_{in}) and the vesicle-membrane/substrate distance (h) for a typical experimentally relevant value of the outer buffer (= 1.332) and wavelength of 546 nm. The white line indicates, for each n_{in}, the h corresponding to the minimum of the intensity (h_0); see Eq. 2.

varying from 0 to 400 nm. As can be seen, for $n_{in} = n_{out} = 1.332$, the intensity minimum occurs at a height of 50 nm. Fig. 2 illustrates the dependence of h_0 (defined as the height corresponding to the intensity minimum) on the refractive indices of the outer and inner buffers.

Validation of the three-interface RICM

To validate experimentally the predictions of the previously described three-interfaces formalism, vesicles adhering unspecifically to the substrate and filled with buffers of known refractive indices are observed (Fig. 3). Since the vesicles adhere tightly (observed membrane fluctuation of the order of the background noise; see paragraph on fluctuations below), h in Eq. 1 is set to zero. The refractive index of the outer buffer (n_{out}) and of the vesicle solution (inner buffer, n_{in}) are measured with a refractometer. Using $h = 0$ and the measured value of n_{out}, the value of n_{in} is calculated and compared to the true value (measured with the Abbe refractometer). The value measured with RICM compares very well with the real value (Table 1).

Height reconstruction of the adhesion disk

Raw RICM images are corrected for inhomogeneous illumination by a background subtraction procedure. The pixels corresponding to the vesicle itself are masked and the rest of the image (consisting of the blank but inhomogeneous background) is fitted with a parabolic surface. The fitting parameters are used to generate the corresponding surface for the entire image including the masked area. This surface is then subtracted from the whole image. This yields an image with a uniform background as judged by comparing the intensity distribution in 20×20 pixels regions at the four corners of the image. The average of N (typically $N = 10$) such images is considered for further analysis. The intensity of each pixel in the averaged image is normalized with respect to the average background intensity. This gives a map of R_{norm} corresponding to the RICM image. For given values of the outer and inner media refractive indices, and using Eq. 2, the membrane height h is calculated at each pixel of the image.

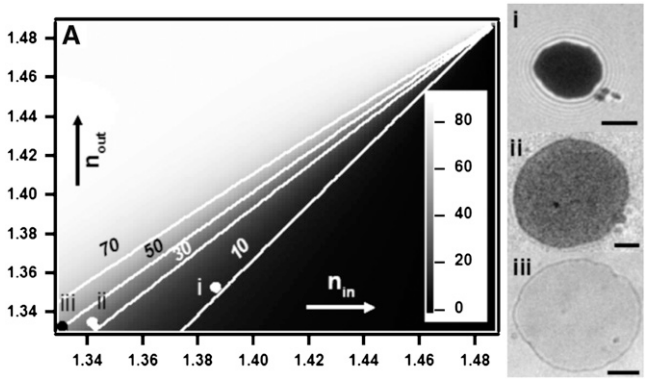

FIGURE 2 Plot of the membrane-substrate distance (h_0) corresponding to the minimum of the intensity (see also Fig. 1 and Eq. 2) for various values of outer (n_{out}) and inner (n_{in}) buffer refractive index, and an illumination wavelength of 546 nm. The white lines correspond to contours of equal h_0 (= 10, 30, 50, and 70 nm). As can be seen, if n_{in} is high and n_{out} is low, the adhesion disk should be dark, since the intensity minimum occurs at a very low height. However, as the refractive index of the inner buffer decreases toward that of the outer buffer, the adhesion disk is expected to look progressively brighter. Moreover, a dark ring is expected to show up surrounding the adhesion disk that traces the height corresponding to the intensity minimum (for example, for $n_{out} = 1.332$ and $n_{in} = 1.342$, this height should be ~30 nm). The panels *I*, *II*, and *III* are RIC micrographs of DMPC vesicles filled with different buffers (and hence exhibiting different refractive indices), immersed in a buffer with refractive index ~1.334, adhering tightly to protein-coated glass. The corresponding points are marked on the plot. Scale bars = 3 μm.

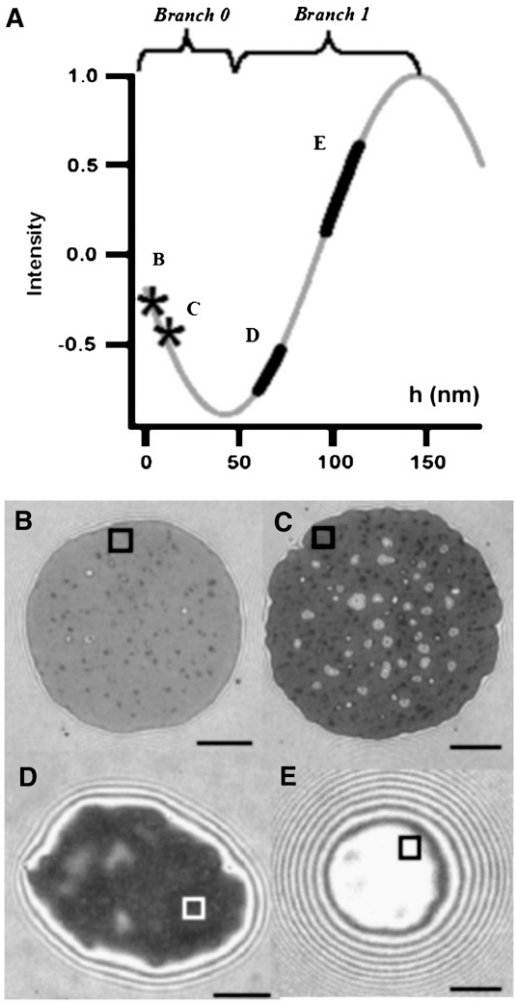

FIGURE 3 (*A*) The theoretically expected intensity as a function of membrane-substrate distance (h) for given n_{in} and n_{out} (= 1.3331 and 1.3366, respectively) branch 0 and branch 1 of the sinusoid (see Eq. 2) are marked. (*B–E*) RIC micrographs of vesicles resting at different heights and as a consequence exhibiting different contrasts. (*B*) On avidin (no polymer cushion) and (*C*) on a sparse hyaluronan cushion (coupling via avidin), the vesicle adheres strongly. The height, indicated by * on the graph, is calculated in branch 0. The height fluctuations are of the order of the background noise (both typically measured inside a small region of interest as shown in the figure). (*D* and *E*) On thick hyaluronan cushion coupled via PLL-80 (*D*) and via PLL-300 (*E*). The heights ± SD calculated in branch 1 are for panel *D*, 66 ± 6 nm; and for panel *E*, 105 ± 8.7 nm. The height fluctuation corresponding to boxes *D* and *E* are marked as thick lines on the theoretical curve. The respective inner and outer buffer are the same in each case, leading to similar reduced volumes. Scale bar = 5 μm.

Since the height is a sinusoidal function of the intensity, the phase $4\pi n_{out}(h - h_0)/\lambda$ in Eq. 2 is determined only modulo π, leading to the need to consider different branches as depicted in Fig. 3 *A*. When the membrane height is below h_0 (for our experimental conditions, $n_{out} = 1.3331$ and $n_{in} = 1.3366$, h_0 is 40 nm), the 0^{th} branch of the sinusoid has to be used. This is the case for vesicles adhered to avidin or avidin-coupled HA (Fig. 3, *B* and *C*). When the membrane height is between h_0 and $h_0 + \lambda/2n_{out}$ (142 nm), the first

TABLE 1 The refractive index of the vesicle inner-buffer measured by bulk refractometry (col. 3) and by RICM (col. 4)

	Inner/outer buffer	Refractive index (refractometer)	Refractive index (RICM)
I	Sucrose-conc./PBS-conc.	1.386	1.385 ± 0.002
II	Sucrose/PBS	1.342	1.340 ± 0.002
III	Glucose/PBS-diluted	1.332	1.327

Inner/outer buffer pairs of concentrated-sucrose/PBS + KCl, normal-sucrose/PBS and glucose/diluted-PBS (see Materials and Methods) are listed in rows *I*, *II*, and *III*, respectively, corresponding to numbers in Fig. 2 *A*. The vesicles have comparable reduced volumes.

branch has to be used. This is the case for vesicles adhered to PLL-coupled HA (see Fig. 3, *D* and *E*). If the membrane height is above $h_0 + \lambda/n_{out}$ (245 nm, third branch or higher), a second wavelength for the incident light has to be employed to ascertain which branch to use for the height calculation (26) (example in Fig. 8). However, to distinguish between branch 0 and 1, information from one incident wavelength is enough. This is because, if the adhesion disk is below the relevant h_0, a dark ring (corresponding to membrane height $= h_0$) surrounds the adhesion disk (see Fig. 2 *A*, *II* and *III* and Fig. 3, *B* and *C*). If, however, the adhesion or contact zone is at or slightly above the relevant h_0 there is no darker rim around it (see Fig. 3 *D*).

Estimation of height fluctuations

Height fluctuations of the membrane in the contact and/or adhesion zone are an indication of the degree of adhesion. In totally adhered vesicles, the membrane hardly fluctuates. In nonadhered vesicles, on the other hand, there are pronounced fluctuations. In RICM experiments, a qualitative absence of fluctuation is often employed to diagnose binding. Here, we have quantified the fluctuation using the following protocol: a series of N images (typically 100) are considered. The background is subtracted as described above. The maximum and the minimum intensity in the image is determined (taking into account possible perturbations due to camera noise or presence of pixel size spatial inhomogeneities). The height at each pixel is determined using the conventional analysis of RICM images (24,25). A small area in the adhesion disk is chosen and a histogram of the spatiotemporal distribution of the heights, h, in the box is constructed. This distribution can be approximated as a Gaussian of the form $Ae^{(h-\bar{h})^2/\sigma h}$. The heights are presented as $\bar{h}\pm\sigma_h$ and $2\sigma_h$ is taken to be the fluctuation. The procedure is straightforward when the heights are confined to one given branch of the sinusoidal function (see discussion above and Fig. 3). However, when fluctuations drive the membrane over an extrema, the estimation is more complicated and a full analysis is beyond the scope of this article. When $2\sigma_h$ is of the order of the expected noise (see also discussion under error estimation), the vesicle is deemed to be adhered.

TABLE 2 Overview of the data for comparison of vesicle adhesion to avidin (*Avi*, col. 2) and to thin hyaluronan cushion (coupled via Avidin, *Avi+HA*, col. 3)

	Avi	Avi+HA
Average height (nm)	3.4 (±0.4)	9.7 (±3.7)
Roughness index (nm)	9 (±3)	17 (±9)
Blister fraction	1.6%	6.8%
Contact angle (rad)	0.54 (±0.04)	0.47 (±0.06)
Spread in contact angle	5%	10%
Adhesion-energy density (μJ/m^2)	1.2 (±0.2)	0.54 (±0.2)
Spreading time (s)	0.45 (n = 18 vesicles)	20 (n = 12)
Spreading velocity (μm/s)	66 (range: 15–120)	8 (0.1–30)

The rows are: average height in the adhesion disk (not including blisters of height above 40 nm); the roughness index of the adhesion disk, calculated for each vesicle as SD of the height in the adhesion disk (also see text); the fraction of the area in the adhesion disk that is under blisters (this is another indication of the roughness); the contact angle; the spread in the contact angle (calculated for each vesicle by taking SD of the angle along the perimeter and expressing it as percent of the average angle); average adhesion energy density; the saturation spreading time; and the spreading velocity. All the values are averages of six vesicles, except for the spreading time and spreading velocity, which are averages of ~15 vesicles. The ''errors'' given in parentheses are the standard deviation of the six values used to calculate the averages and are an indication of how much the values differ from vesicle to vesicle. Note that the roughness, the blister fraction, and the spread in contact angle are all higher in the Avi-HA case.

Height of fringes, contact angle, and contact length

The adhesion disk is identified by tracing the first bright fringe using the Snake algorithm implemented in Image-J (29). Using this as a starting contour, radial lines are drawn outwards and inwards from the edge of the adhesion zone and the resulting intensity pattern along the line is stored. For each line, the extrema are identified using self-written routines and information about their position is stored. The expected height corresponding to each extremum is calculated using Eq. 2. A plot of the stored position versus the expected heights gives the height profile of vesicle membrane as it curves away from the substrate. The vesicle profile far from the edge of the adhesion disks tends to a straight line. From this, the contact angle θ and the contact length L is measured (contact length L is defined as the distance from the point at which the membrane adheres to the substrate ($h = 0$) to the point at which the straight line representing the vesicle profile far from the substrate intersects the substrate) (21). Here, one important difference with the conventional analysis is introduced: instead of taking the minimum of the intensity as the zero of the height ($h = 0$), we use the height construction algorithm detailed above to determine the zero. The values θ and L are determined all along the contour of the adhesion disk. Following Sackmann and Bruinsma (21), the values of L and θ are used to calculate the adhesion energy density, W, given by $W = \kappa/L^2(1 - \cos\theta)$, where κ is the membrane-bending rigidity ($= 100\ k_BT$ (19,22)). Finally, the values obtained for all the lines (typically 200–400 points depending on the size of the adhesion disk) are averaged, excluding regions of very high curvature of the contact line. The values reported in Table 2 are further averaged for six different vesicles.

Estimation of errors

The absolute membrane height determination by RICM is mainly limited by two sources of error: the error in the intensity measurement which in turn is dominated by the shot noise of the camera and the error in determining h_0, which arises from error in determination of d_{lipid}, n_{lipid}, n_{in}, or $n_{out.}$. Another error, affecting mainly the contact angle measurement, arises from the planar approximation for the reflecting interfaces.

The first kind of error, coming from the shot noise, is intensity-dependent. For typical intensities in the adhesion zone (averages of over 10 images, corresponding to height <80 nm; Fig. 3, *B–D* and Fig. 6, *B* and *C*), the standard deviation of the height, due to the noise, ranges from 1.5 to 2.5 nm. For a contact zone corresponding to a height of ~100 nm (Fig. 3 *E*), this value is 4 nm. This error affects both the relative and absolute height determinations.

The second kind of error, from the uncertainty in refractive indices and the membrane thickness, affects only the absolute height—the relative height differences are not affected by this. The reflective index of the vesicle membrane is taken from Radler and Sackmann (24), where it was determined for a lipid bilayer consisting of DMPC. If an error of 1% (1.486 ± 0.02) in

the lipid refractive index or an error of 25% (5 ± 1 nm) in the membrane thickness is assumed, the resultant error in determining h_0 is 3 nm. Uncertainty also arises from the refractive index of the hyaluronan cushion, which may be different from the refractive index of the outer buffer and may even change due to compression of the HA by the vesicle. Benz et al. (9) shows that, at a concentration of 4 mg/ml, the refractive index of HA begins to differ appreciably (>1%) from that of water. In this experiment, the unperturbed density of HA is ~160 μg/ml close to the surface (see Results) and therefore the refractive index is essentially that of the buffer. For this initial density, the layer has to be compressed to <4 nm for the refractive index increase to be relevant here. Thus, we can assume that the variation of the refractive index of the cushion from that of water is negligible. The uncertainty in the determination of the refractive index of the inner buffer (n_{in}) is compounded by the fact that strongly adhering vesicles may leak and exchange buffer with the outside, thus changing n_{in}. Here, for vesicles adhering to bare avidin-coated surfaces, we determined n_{in} assuming $h = 0$ and found that n_{in} does not change appreciably from its initial value after adhesion. Thus it can be safely assumed that there is no leakage. Using Fig. 2, for the values of $n_{out} = 1.332$ and $n_{in} = 1.336$ the error in determination of h_0 is 3 nm for a mistake of 0.002 in one of the refractive indices.

The third type of error arises from the fact that for the RICM analysis, we use the simple theory that takes into account only the normally incident light rays reflecting from planar interfaces. The error introduced in the determination of the height within the contact zone, where the membrane is essentially flat, is negligible. However, taking into account the non-normal rays, the curvature of the interfaces may shift the estimated contact angles by a factor that depends on the real value of the contact angle (25). This underestimation of the contact angle has always been ignored in the context of vesicles and it is beyond the scope of this article to account for it. However, assuming a 40% error in the contact angles, in this case the calculated adhesion energy density shifts by a factor of ~2 for both no-polymer and sparse polymer case (since apparent angles are of comparable values in the two cases). Thus it is legitimate to use this method to compare adhesion energies.

To summarize, the typical error in determining the absolute height in the adhesion disk, which includes the error from determination of h_0 as well as from the determination of the relative height, is ~4 nm.

RESULTS

Characterization of the hyaluronan cushion by colloidal probe interference microscopy

The thickness and homogeneity of the polymer cushion formed via avidin (avi-HA) and via PLL-300 (PLL300-HA) are estimated by measuring the heights of colloidal beads resting on the cushions. Adapting the procedure described in Schilling et al. (26) to a population of beads, we determine the absolute height of the particles in the 0–200-nm range above the glass substrate. The distribution of time-averaged measured heights is shown as a histogram (Fig. 4), revealing a significant difference between average (mean ± SD) of heights of the beads on avi-HA cushion ($h = 67 \pm 39$ nm) and PLL300-HA cushion ($h = 83 \pm 27$ nm). These measured heights reflect the thickness of the underlying cushion but may differ from the real thickness because of a slight compression of the cushion by the beads (26). The width of each distribution gives an indication of the spatial heterogeneity of the cushions. The data indicate that avi-HA cushions are thinner as well as more sparse and inhomogeneous than the HA-PLL300 cushions.

Estimation of the concentration of bound hyaluronan by confocal microscopy

The amount of bound hyaluronan is estimated using scanning confocal microscopy by comparing the fluorescence of bound fluorescently-labeled hyaluronan (fl-HA) cushion with the fluorescence of a reference sample. The reference is a bulk solution of a mixture of HA and fl-HA at a total HA concentration of $c_0 = 10$ μg/ml. The sample is scanned at random places along horizontal lines at heights spaced by $\Delta z = 0.5$ μm, leading to a measured profile of fluorescence perpendicular to the substrate. The surface density C_S of fl-HA was calculated as $C_s = c_0(I/I_0)$, where $I = 1350 \pm 100$ is the fluorescence of the cushion integrated along the vertical direction, z, minus the value of the background intensity; and $I_0 = 85.7$ is the fluorescence from an equivalent plane in the reference, calculated by deconvolving the out-of-focus contributions. From this, we obtain $C_S \sim 16$ μg μm/ml leading, for a 100-nm-thick cushion, to a concentration of ~157 ± 10 μg/ml. The differences between the avidin and PLL cases are within the experimental error.

Description of vesicle adhesion

The vesicles, which are floppy and roughly spherical (or spheroidal), settle under gravity (because of the difference in

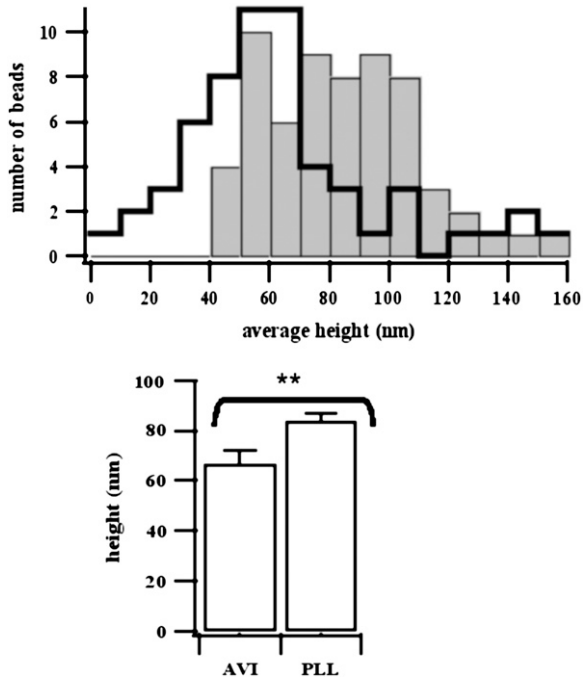

FIGURE 4 Distribution of the heights of colloidal beads (10 μm diameter) lying randomly on hyaluronan cushions as measured by RICM. (*Top*) HA is coupled to glass via avidin (*open bars*) or PLL-300 kDa (*shaded bars*). The height of a single bead is measured over 100 time frames and ~60 beads are considered for each sample. (*Bottom*) Mean average ± SE of height distribution. The HA cushion is significantly thicker and more homogeneous when coupled through PLL than avidin (the averages are statistically different as tested by unpaired *t*-test).

specific gravity of the inside sucrose buffer and the outside PBS buffer) on substrates that are either coated with a protein or exhibit a polymer cushion. The vesicles are initially non-adhered and their subsequent fate depends on the presence or absence as well as the thickness of the underlying polymer cushion. After adhesion, they assume a truncated spheroidal shape (22).

As qualitative description of the adhesion obtained by visual inspection of the RICM movies, two categories of interactions can be identified (Fig. 3): 1), the membrane does not fluctuate (fluctuation comparable to camera noise) and exhibits large patches that are close to the substrate ($<\sim$10 nm) henceforth referred to as ''adhered''; and 2), the membrane fluctuates (fluctuation significantly more than camera noise) and resides at a non-zero height (average membrane-substrate distance in the contact zone $>\sim$40 nm), henceforth referred to as ''nonadhered''. We verified that vesicles exhibiting low fluctuations fail to detach under a gentle hydrodynamic flow.

Both DMPC and biotin vesicles adhere tightly to bare glass coated with either PLL or avidin. Moreover, with respect to all the properties discussed below (for example: contact angle, roughness of adhesion disk, spreading kinetics, etc.), DMPC and biotin vesicles behave in the same way. This is also true in the presence of a hyaluronan cushion. These observations strongly indicate that the vesicle substrate interaction is dominated by unspecific forces. The results presented below are valid for both DMPC and biotin vesicles and no further distinction is made between them.

Tuning the membrane-substrate distance

On a bare substrate (no-cushion) or on HA attached via avidin (thin-cushion), the vesicles adhere. However, there are quantitative differences, discussed later, between the two cases. HA coupled to PLL, on the other hand, gives rise to thicker layers and prevents adhesion of the vesicle to the substrate. The vesicle-membrane height depends on the molecular weight of the PLL used for the coupling. On HA bound via PLL-80 kDa, the vesicles are low ($\sim$65 nm) but still fluctuate (Fig. 3 *D*). On HA bound via PLL-300 kDa, the vesicles reside at a height of $\sim$100 nm and fluctuate considerably. Fig. 5 gives an overview of the proportion of adhered (defined as fluctuation $\sim$ noise) vesicles in a population for all the cases described above.

Vesicle on thin-cushion versus no-cushion

In the absence of a polymer cushion or in the presence of a thin-cushion the vesicles adhere. There are characteristic differences in the state of adhesion depending on the presence or absence of the polymer, which are summarized in Table 2 and detailed below.

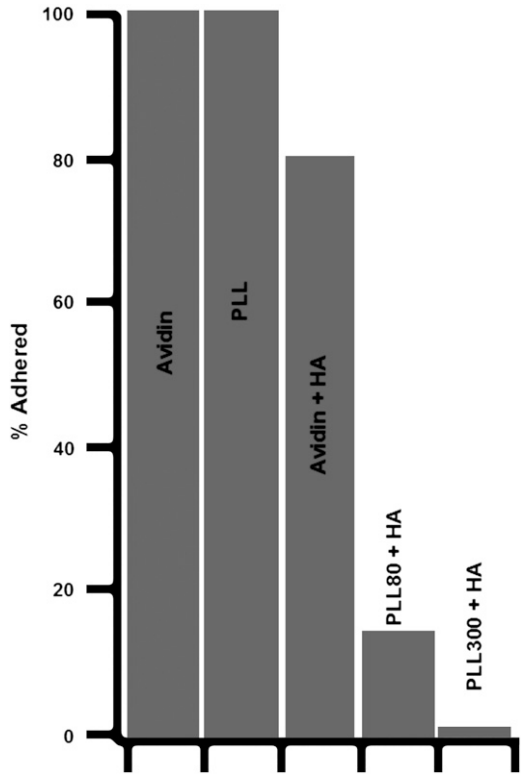

FIGURE 5 Proportion percentage of adhered vesicles (according to fluctuation criterion; see text) 30 min after the addition of vesicles into observation chamber for the following substrates: avidin ($N = 50$ vesicles), PLL ($N = 10$), avidin+HA ($N = 50$), PLL-80+HA ($N = 10$), and PLL-300+HA ($N = 50$). On bare avidin and PLL (case: no-cushion), all the vesicles adhere. On PLL-300-HA (case: thick-cushion) none of the vesicles adhere. On PLL-80-HA, most vesicles do not adhere; and on avidin-HA (case: thin-cushion), most, but not all, vesicles adhere.

The adhesion disk

Fig. 6, *A* and *B*, illustrates typical RICM images for the cases of a vesicle adhering to a bare avidin substrate and to a thin hyaluronan cushion. The corresponding maps of height distribution is shown in Fig. 6, A' and B'. In case of no-cushion, the adhesion disk is fairly homogeneous and the average height ($\pm$SD for six vesicles) within the adhesion disk is 3.4 $\pm$ 0.4 nm. Similar results are obtained on bare PLL (data not shown).

For the case of a vesicle adhering to a thin hyaluronan cushion adsorbed to an avidin substrate, the adhesion disk is inhomogeneous. A large part of the membrane is close to the surface at an average height ($\pm$SD for six vesicles) of $\sim$10 $\pm$ 4 nm. However, bubbles or blisters whose heights greatly exceed that of the surrounding homogeneous disk are visible (*white arrows* in Fig. 6 *B*). In addition to the bright blisters, the RIC micrographs also show dark spots which are blisters that happen to have a height close to h_0 (40 nm in this case). Inspection of a large number of vesicles reveals that the blisters can vary from few tens of nm to a few hundred nm in height and are a few μm in lateral size. To quantify the

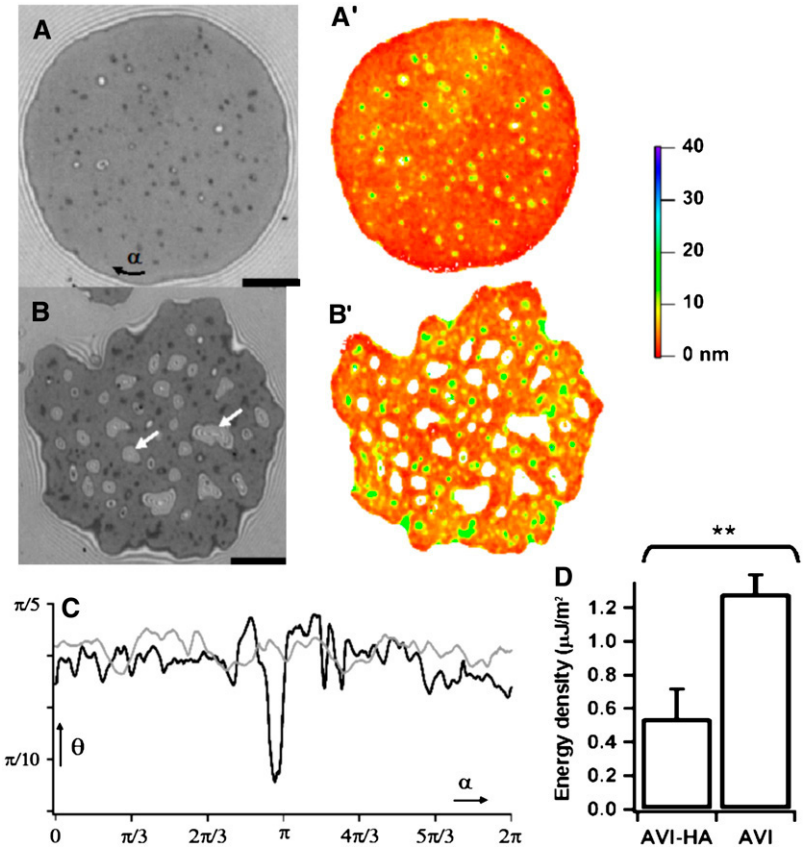

FIGURE 6 (*A* and *B*) RIC micrographs of vesicles adhered to substrates coated with avidin and with hyaluronic acid coupled via avidin (avi-HA). *A′* and *B′* are the corresponding average height maps determined using branch 1 of Eq. 2 (see also Fig. 4). The color represents vertical height that goes from 0 to 40 nm. The parts of the membrane that are higher than 40 nm (where the height calculation should be done in another branch), are painted white. Note that the dark patches in RIC micrograph (with intensity lower than the average intensity in the adhesion disk) correspond to larger heights. (*C*) The spatial distribution of the contact angle along the rim of the adhesion disk for substrates coated with avidin (*shaded*) and with avi-HA (*solid*). (*D*) Adhesion energy density (mean average ± SE of distribution) on substrates coated with avidin and with hyaluronic acid coupled via avidin. (Unpaired *t*-test reveals significant difference.) Scale bar = 5 μm.

occurrence of blisters, we define them as regions of the membrane where the height is more than an arbitrarily chosen cutoff (= 40 nm for convenience arising from optical considerations). Defining blisters as parts of the adhesion disk with height >40 nm, it can be seen that on the average, 7% of the adhesion disk is covered with blisters in case of vesicles on thin HA and only 1.6% in the no-polymer case. The cutoff of 40 nm can be varied by ~20% without seriously affecting this result. To determine the height of membrane in the blisters quantitatively, the value of the phase in Eq. 2 has to be chosen properly. Since this value changes within each blister (as fringes are crossed), this is a nontrivial task beyond the scope of this article. However, to objectively compare the roughness in the polymer and no-polymer cases, we define a roughness index by setting the height of all blisters to 40 nm and calculating the SD of the membrane height in the adhesion disk. This roughness index is 17 nm for the thin polymer case and 9 nm for the no-polymer case (see Table 2 for an overview of the above discussed data).

Contact angle and adhesion energy

As is evident from comparing Fig. 6, panels *A* and *B*, the edge of the adhesion disk is markedly more jagged in the case of spreading on a thin-polymer layer as compared to the no-polymer case. This is also reflected in the variation of the measured contact angle along the perimeter (Fig. 6 *C*): the spread in contact angle is 4% in the no-polymer case and 12% in the thin-polymer case for the case of vesicle depicted here (see Table 2 for statistical overview of data). Following Sackmann and Bruinsma (21), the adhesion energy density (W) can be estimated from the contact angle and contact length (see also Materials and Methods, and Discussion). Comparing the averages reveals that W is significantly lower ($p = 0.005$) in the presence of the polymer (Fig. 6 *D* and Table 2).

Spreading kinetics

The time evolution of the adhesion disk area is depicted in Fig. 7 *A*, which shows two typical curves of growth of area as a function of time (see also Supplementary Material for movies of spreading vesicles). The adhesion area increases and saturates to a maximum value. We define the time to reach this plateau as spreading time or saturation time (T_{sat}). It is defined as the time after which the difference in the adhesion area between two time frames is <5% of the total area at saturation (indicated by an *arrow*). Data (Fig. 7 *B*, Table 2) shows that the saturation time is approximately an order-of-magnitude larger when vesicles adhere through a thin polymer cushion. In case of spreading on a bare substrate, the saturation time is largely correlated with the GUV size; larger vesicles take longer to spread (Fig. 7 *B*). However, in

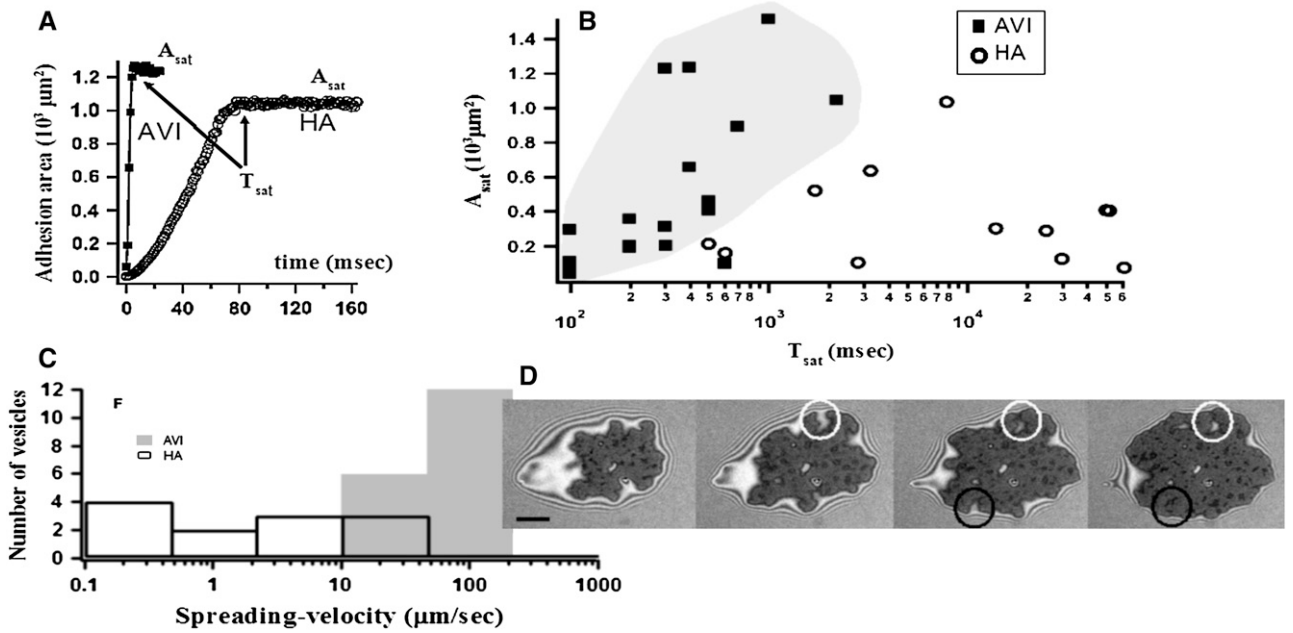

FIGURE 7 (*A*) Typical growth curves for the adhesion disk area for substrates coated with avidin (*solid squares*) and with hyaluronic acid coupled via avidin (*open circles*). The saturation spreading times (T_{sat}) are indicated by arrows. (*B*) Overview of T_{sat} for vesicles spreading on avidin (*solid squares*) or hyaluronan-coupled-via-avidin (*open circles*). In the former but not in the latter case, a strong correlation between the adhesion disk area and the saturation times is seen (relevant part of the graph is shaded as a guide to the eye). The vesicles have similar reduced volumes. (*C*) Histograms of spreading velocity (defined as $\sqrt{A_{sat}}/T_{sat}$) calculated with logarithmic binning. (*D*) Time-lapsed RICM of a vesicle adhering to a hyaluronan coated (via avidin) surface. Two developing blisters are indicated by a white circle and a black circle. At later times one forms a white blister (*white circle*) and the other a black patch (*black circle*) that are both higher than the surrounding shaded adhesion disk. Time between frames = 19.6 s, scale bar = 5 μm.

the case of spreading through the thin HA layer, the correlation between the spread time and radius is not apparent, probably because the inhomogeneity of the substrate plays a more significant role and masks the size dependence. It should be noted that all the vesicles are subjected to the same osmotic balance (same inner and outer buffer) and are thus expected to have comparable initial reduced volumes. The spreading velocity (defined as $\nu_r = \sqrt{(A_{sat})}/T_{sat}$, where A_{sat} is area at saturation), shows no size dependence. The spreading is significantly slower on the thin-cushion compared to the no-cushion case (Fig. 7 *C*). The average spreading velocity on bare avidin is 66 μm/s (range: 15–120, SD: 22) and on the thin-HA layer it is 8 μm/s (0.1–30, SD: 10).

An interesting aspect of the spreading process on the thin-HA cushion is the formation of the blisters. As depicted in Fig. 7 *D*, the blisters frequently arise from ''fjords'' that are formed when the membrane adhesion proceeds faster on both sides of such a structure than along the structure itself. The adhering segments subsequently rejoin leaving an island of elevated blister that shows up as a bright (or dark) patch. This progression of events indicates that the blisters may correspond to patches on the cushion which are less amenable to compression (see also discussion on fate of the HA) than the rest of the cushion due to locally elevated concentration of the HA. Some of the blisters also arise spontaneously, without any preexisting HA-fjord. At later times, the blisters may fuse and merge to form larger blisters (as visible on Fig. 8 *A*).

Fate of the HA-cushion upon adhesion

The fate of the hyaluronan cushion upon vesicle adhesion was inferred from experiments with fluorescently labeled HA-cushion. The adhesion disk of the vesicle was identified from interference reflection microscopy images (interference reflection microscopy is RICM without contrast enhancement by an antiflex objective; the contrast is consequently poorer). The corresponding fluorescence images exhibit a uniform intensity (Fig. 8). This indicates that the hyaluronan is neither expelled from the adhesion disk nor gathered significantly in the blisters. Since the fluorescence signal is weak and the dye bleaches fast (within few hundreds of milliseconds), a further quantitative study is not possible at this stage.

Vesicles doped with short polymers

Vesicles decorated with 5% PEG-2000 chains (diameter of gyration ~4 nm (30,31)) adhere strongly to both avidin- and PLL-coated surfaces (data not shown). No qualitative difference is introduced by the presence of PEG. In contradiction to earlier reports (15,18), in this case, the unspecific adhesion is not entirely screened by the PEG. The discrepancy is probably a result of absence of additional blocking agents (like bovine serum albumin). However, in agreement with Boulbitch et al. (18), the PEG slows down the spreading kinetics. On a thick

HA layer (via PLL-300), the PEG vesicles do not adhere. Again, no qualitative difference is introduced by the presence of PEG.

On a sparse HA layer coupled via avidin to the glass substrate, the vesicles either do not adhere at all or assume a hitherto unreported configuration of partial adhesion where the adhesion zone spans only a part of the contact zone. For example, in Fig. 9 only 5% of the contact zone is tightly adhering. In such cases of partial adhesion, the adhesion zone expands very slowly over several hours but never extends over the whole contact zone over this timescale.

Enzyme treatment

Treatment of thick HA layers (coupling via PLL-80) with the hyaluronic acid lysing enzyme hyaluronate lyase destroys the HA cushion (32). If vesicles are added afterwards, they exhibit fast adhesion and a uniform adhesion disk, as in the no-polymer case. Addition of the enzyme to an HA-PLL cushion with nonadhering vesicles also leads to fast and tight adhesion (Fig. 10). The average saturation time is 250 ms ($n = 9$ vesicles), which is comparable to the saturation time in the no-polymer case.

DISCUSSION

Absolute height measurement from RICM analysis

The RICM formalism developed here, which takes into account the refractive indices of the various layers, has important implications for analysis of data from vesicles. Our results show that it is definitely required for quantitative measurement of membrane-substrate distance. Even for a qualitative interpretation, the conventional assumption that the minimum of the intensity corresponds to the minimum of the height is insufficient. For example, often the intensity of an adhesion patch is seen to decrease as the vesicle goes from first contact to fully spread (see for example Fig. 2 of (11)), and the equilibrium adhesion disk is sometimes surrounded by a dark rim (see figures in (9) and (10)). These features were usually ignored in previous studies, but can be explained in light of the formalism presented here.

In the case of cells, the typical cytoplasmic refractive index is ~1.384 (33). Taking the refractive index of the outer medium to be 1.340 (slightly larger than PBS to account for

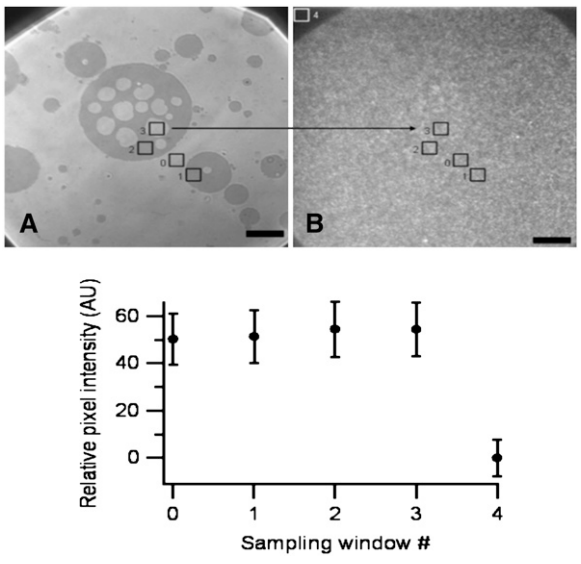

FIGURE 8 Reflection (*A*) and fluorescence (*B*) micrographs of the same region of a sample prepared with fluorescent HA: biotin HA (1:1) cushion-coupled to glass via Avidin and on which vesicles are adhering. Five regions of interest (ROI) are delimited. (*C*) Average fluorescence intensity (±SD) in each ROI relative to ROI #4 showing that there is no significant change in fluorescence whether the ROI is located on the adhesion zone of a vesicle, on a blister or outside an adhesion zone. Scale bar = 10 μm.

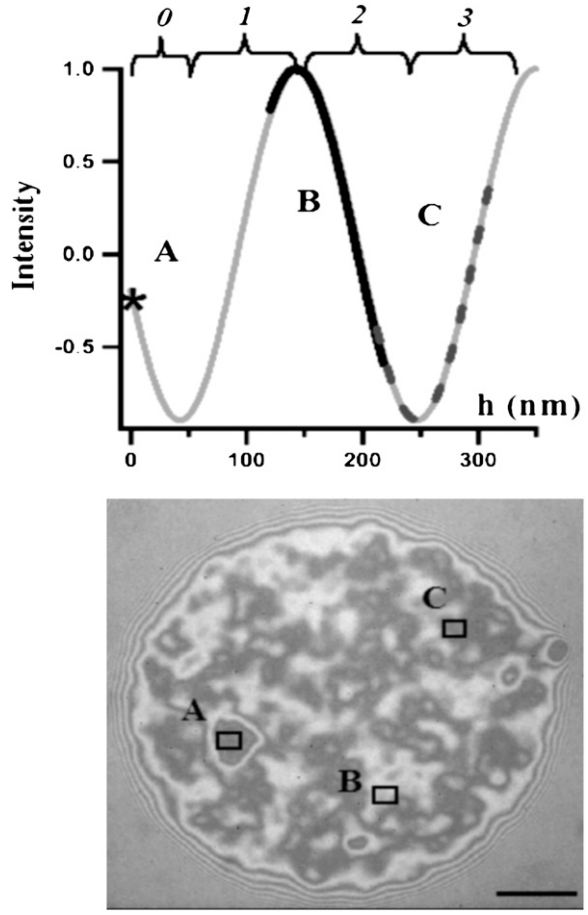

FIGURE 9 The theoretically expected intensity as a function of membrane-substrate distance (h) for given n_{in} and n_{out} (= 1.332 and 1.342, respectively) and RIC micrograph of a vesicle decorated with PEG partially adhered on a substrate with thin hyaluronan cushion. At patch *A*, the membrane height is at the limit of the instrument resolution and the height fluctuation is of the order of the noise (marked by * in the sinusoid). At patch *B*, branch 2 of the sinusoid (see Eq. 2) has to be used, and the height ± fluctuation is 170 ± 50 nm (*thick line*). At patch *C* (height 260 ± 50 nm, *dashed line*), branch 3 is used. For determining the relevant branches for the free part of the membrane, two-color RICM (wavelengths 546 nm and 436 nm) was used. Scale bar = 12.5 μm.

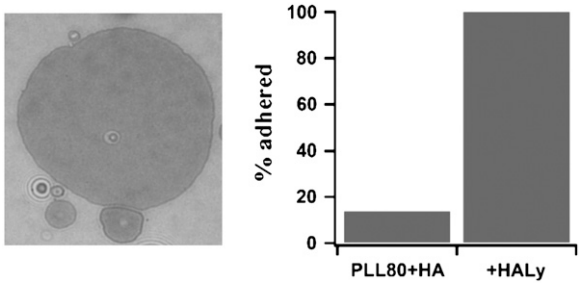

FIGURE 10 (*Left*) A typical example of the adhesion disk of a vesicle adhering to a substrate coated with HA coupled via PLL-80 and subsequently treated with hyaluronate lyase. (*Right*) Percentage of vesicles adhered after 1/2 h in the presence (+HALy) and the absence (PLL80+HA) of added hyaluronate lyase (10 vesicles each).

dissolved proteins) and referring to Fig. 2, it can be seen that the darkest patches should correspond to membrane-substrate distance of ~10 nm. However, presence of high amounts of dissolved proteins, particularly albumins, in the medium can elevate its refractive index considerably—an increase to 1.366 would imply a distance of 20 nm for the intensity minimum. Furthermore, the presence of material from the extracellular matrix or the glycocalyx, whose refractive index may be fairly high, can enhance this effect. On the other hand, presence of elevated amounts of actin in the cytosol, for example because of stress fibers, can drive up the refractive index of the inside and shift the patch height for minimum intensity to lower values. The obvious implication is that concentrating actin above a patch is enough to make it look darker without actually changing the membrane-substrate distance. Thus the apparent height is highly influenced by the refractive index of the medium and cell surface polymers as well as local refractive index of the cytosol; therefore even qualitative estimates should be made cautiously. In principle, with the knowledge of the refractive index of the medium and the cytosol, the distance corresponding to the darkest patch either can be read from Fig. 2 or calculated using analytical expression given in the Appendix.

Biomimetic relevance of hyaluronan cushions

We set up the vesicle and HA-cushion system to mimic early stages of cell adhesion which, in many cases, is known to be modulated by the presence of HA (1,4,8). We used giant unilamellar vesicles to mimic the cells and surface-supported cushion of hyaluronan to mimic the pericellular coat. To focus on the ability of hyaluronan to block unspecific interaction, no additional blocking agent (bovine serum albumin, fat-free milk, or casein) was used. Since hyaluronic acid is a polyelectrolyte, its configuration is highly sensitive to the ambient ionic strength. All the experiments reported here were carried out at physiological salt concentration to ensure a physiologically relevant configuration for the hyaluronan.

Hyaluronan has been detected on the surface of many cells, including epithelial and endothelial (8,34,35) cells, keratinocytes (36), muscle cells, and certain immune cells (37). However, the organization of the HA coat, in particular, the thickness, is not characterized for many cells. From the data in literature, it is clear, however, that the thickness of the pericellular coat varies considerably from cell type to cell type and also during the lifecycle of the cell. For example, in endothelial cells it is approximately half a micron (35); in epithelial cells, ~μm (8); in chondrocytes, ~3 μm (38,8); and in resting smooth muscle cells, it is negligible, whereas in the same cells, while migrating, it can be ~10 μm (39). We show here that artificial HA cushions (that are up to 10 times thinner than the typical pericellular coat) can prevent adhesion of vesicles to the substrate. Interestingly, a thin (~60 nm) layer of hyaluronic acid, which is also relatively inhomogeneous (width of height distribution ~40 nm; see Fig. 4), allows adhesion but strongly alters both the equilibrium state and the adhesion kinetics compared to the case where no polymer is present.

An additional property of the biomimetic HA cushions described here is that they are very soft (~200 Pa (11)). It has been shown that cells not only change their morphology in response to the compliance of the substrate but even their differentiation may be dependent on the softness of the substrate they grow on (40). Thus the thickness-tunable HA cushions reported here represent a promising material for preparation of ultrasoft substrate of tunable compliance (41).

Redistribution of hyaluronan and blistering phenomenon

The question of the redistribution of surface hyaluronan (or more generally any cell surface polymer, including the glycocalyx (23)) during adhesion is an important issue that is poorly understood. Clearly, in cells, before ligand-receptor mediated adhesion can occur, the thick hyaluronan layer has to be expelled from zones of close contact between membrane and substrate. The group of Addadi has been able to follow this redistribution during the process of spreading of chondrocytes on fibronectin and show that the hyaluronan, tagged with 200-nm quantum dots, gets trapped in blisterlike structures (4). Interestingly, these blisterlike structures are reminiscent of the structures observed in this work in the vesicle/thin-polymer layer case. However, in this case, fluorescence measurements indicate that even in those areas of the adhesion disk that are apparently in close contact with the substrate (~10 nm), HA is still present. This is not as surprising as it sounds because once the water associated with the swollen hyaluronan is squeezed out, the polymer occupies very little space (for example, a thickness of 0.3 nm for HA films is reported in (42)). In fact, it is conceivable that once the hyaluronan is compressed enough to condense the counterions, further compression of the neutral polymer is easier.

Blisters similar to those seen here have been reported previously under two very different circumstances:

1. A charged vesicle adhering to a charged substrate exhibits blisters as a result of accumulation of counterions (14). In this case, the charge on the vesicle is very weak (DMPC) and the blister formation on bare avidin is very low. Unlike in the case of ion accumulation, the observed blisters are often not tense and may exhibit thermal fluctuation (data not shown). The self-repulsion of the hyaluronan probably contributes to the formation of the typical distorted hemispherical shape of the blisters (as seen in Fig. 6).
2. When the membrane is doped with 1% of PEG lipids, blisters of height $<\sim$100 nm are seen (18). In this case, the blister dynamics is very similar to the case shown in Fig. 7 *D*, and also begins as a fjord during the spreading process. However, in case of PEG, the blister heals over timescales of few seconds indicating that the PEG is eventually expelled from the adhesion disk. In this case, blisters do not heal; often they coalesce to form larger blisters.

The thin polymer layer presents a rather inhomogeneous surface (see height distribution in Fig. 4) and as a result, the adhesion disk is also highly inhomogeneous in terms of the membrane height (presence of blisters), the overall shape, and the distribution of the contact angle. The irregular shape of the adhesion disk is reminiscent of spreading of vesicles on chemically patterned surfaces (43), where it was shown that the shape of the adhesion disk can be influenced by the surface patterns.

The calculation of adhesion energy density from the contact angle is legitimate only when the contact curvature of the membrane is larger than the local curvature of the contact line of the adhesion disk (21). Because of the irregular shape of the adhesion disk in the case of the thin polymer, this criterion is sometimes locally violated. Therefore, for the adhesion energy density presented in Fig. 6 and Table 2, the averaging was done only in those stretches along the perimeter of each vesicle where the above criterion is fulfilled. The presence of the polymer cushion lowers the adhesion energy by approximately threefold. Such lowering of adhesion energy is also observed in the presence of the much shorter PEG chains on the vesicles (18).

Spreading kinetics and viscous role of cell coats

The presence of the polymer cushion slows down adhesion by a factor of 10. From Puech et al. (17), it is clear that such an effect can arise from a change in the adhesion energy (18) and/or a change in the viscosity of the external medium (44). Quantitative analysis following Puech et al. (17) suggests that a 10-fold increase in either the adhesion energy or the viscosity is needed to lower the spreading time by an order of magnitude, as seen here. Thus, the observed threefold decrease in the adhesion energy is clearly not sufficient to account for the slow dynamics. In Benz et al. (9), it is seen that at a concentration of 1–1.5 mg/ml, surface-grafted HA in HA solution has a viscosity of $\sim$10 mPa/s. To reach such concentrations in our system, the HA has to be compressed to $\sim$10 nm, which is indeed achieved in some patches in the adhesion disk. This suggests that the slower observed spreading kinetics is at least in part due to increased viscosity, rather than solely due to reduced adhesion energy.

A redistribution of some elements of glycocalyx (CD43) during early stages of neutrophils spreading has been observed (45) and it has been speculated that such redistribution is responsible for modulation of spreading dynamics (46). In the light of the above discussion, we hypothesize that this modulation is effected, to a significant extent, through a change in the viscosity. However, it should be kept in mind that cell spreading is typically slower than the timescales discussed here. For example, for relatively fast spreading cells like neutrophils, the adhesion zone area changes by $\sim$100 μm^2 in 100 s (46), yielding a spreading velocity for the adhesion zone of $\sim$1 μm/s. On the other hand, the cell coat is typically thicker and may offer higher viscosity than in the artificial system presented here.

Enhancement of repulsive effect with PEG

Neither PEG lipids (5%) alone nor a thin cushion of hyaluronan (via avidin) alone prevents adhesion. However, together, they have an additive effect and do largely prevent the vesicles from adhering. The resulting characteristic partial adhesion (Fig. 8) probably arises because the hyaluronan cushion is rather inhomogeneous. Wherever there is sufficient amount of hyaluronan, the membrane fails to adhere. Patches that are virtually bare of hyaluronan and exhibit only avidin promote membrane adhesion. The scenario is different when there are no PEG lipids in the membrane. In that case, the membrane adheres also to hyaluronan-rich patches by compressing the HA. Thus, (non)adhesion of PEG-rich vesicle membranes can be used to evaluate the quality of hyaluronan coverage. The coexistence of adhesion patches and nonadhesion zones may be promoted by the segregation of the PEG lipids outside the adhesion patches (18).

CONCLUSION AND PERSPECTIVES

We show that in vitro, the mere presence of hyaluronan prevents close contact between membranes even when it is only $\sim$100-nm thick. The effect is intensified in the presence of very short surface-coupled polymers with $\sim$4 nm radius of gyration. It can be expected that, if the strong unspecific interaction with the glass is blocked, a mimetic system can be designed that exhibits competition between the repulsion from the hyaluronan cushion and a specific adhesion between a receptor-coated substrate and counter-receptors on the vesicle. We expect the fate of the intervening hyaluronan layer to remain the same as that reported here. In cells, the

hyaluronan layer is usually much thicker (depending on the cell type) than 100 nm, and therefore cells must have a special mechanism to make membrane-substrate contact, either by partial removal of the hyaluronan or by forcing membrane-substrate contact through the HA (for example by extension of a receptor-bearing membrane finger or microvilli). Upon comparison of our results on vesicles with that of Cohen et al. (4) on cells, it seems likely that the gathering of the quantum-dot-labeled hyaluronan in pockets under the membrane seen in cells arises from a similar mechanism as the blister formation seen here for vesicle membranes. Therefore it can be speculated that cells first partially degrade their hyaluronan coat and then rely on passive compression (and/or displacements) of HA to establish the final contact with the substrate.

APPENDIX

Using Eq. 1 and the intermediate notation

$$\gamma = \frac{r_{23}}{r_{12}}(1 - r_{12}^2); \quad \delta_2 = 4\pi n_2 d_{\text{lipid}}/\lambda,$$

analytical expressions for coefficients A and h_0 of Eq. 2 have been derived:

$$A = 2\frac{r_{12}}{r_{01}}(r_{01}^2 - 1)\sqrt{1 + \gamma^2 + 2\gamma\cos\delta_2},$$

$$h_0 = \frac{-\lambda}{4\pi n_{\text{out}}}\operatorname{atan}\frac{\gamma\sin\delta_2}{1 + \gamma\sin\delta_2}.$$

SUPPLEMENTARY MATERIAL

To view all of the supplemental files associated with this article, visit www.biophysj.org.

We thank N. Kischgessner for help with the Snake algorithm, R. Merkel and P. Bongrand for useful discussions, and P. H. Puech, A. Smith, and P. Bongrand for critical reading of the manuscript.

REFERENCES

1. Cohen, M., D. Joester, B. Geiger, and L. Addadi. 2004. Spatial and temporal sequence of events in cell adhesion: from molecular recognition to focal adhesion assembly. *ChemBioChem*. 5:1393–1399.
2. Alon, R., T. Feizi, C. T. Yuen, R. C. Fuhlbrigge, and T. A. Springer. 1995. Glycolipid ligands for selectins support leukocyte tethering and rolling under physiologic flow conditions. *J. Immunol*. 154:5356–5366.
3. Pierres, A., A. M. Benoliel, and P. Bongrand. 2000. Cell-cell interactions. *In* Physical Chemistry of Biological Interfaces. W. Norde and A. Baszkin, editors. Marcel Dekker, New York.
4. Cohen, M., Z. Kam, L. Addadi, and B. Geiger. 2006. Dynamic study of the transition from hyaluronan- to integrin-mediated adhesion in chondrocytes. *EMBO J*. 25:302–311.
5. Toole, B. P. 2004. Hyaluronan: from extracellular glue to pericellular cue. *Nat. Rev. Cancer*. 4:528–539.
6. Toole, B. P. 1991. Proteoglycans and hyaluronan in morphogenesis and differentiation. *In* Cell Biology of Extracellular Matrix, 2nd Ed. E. Hay, editor. Plenum Press, New York.
7. Allison, D. D., and K. J. Grande-Allen. 2006. Hyaluronan: a powerful tissue engineering tool. *Tissue Eng*. 12:2131–2140.
8. Cohen, M., E. Klein, B. Geiger, and L. Addadi. 2003. Organization and adhesive properties of the hyaluronan pericellular coat of chondrocytes and epithelial cells. *Biophys. J*. 85:1996–2005.
9. Benz, M., N. Chen, and J. Israelachvili. 2004. Lubrication and wear properties of grafted polyelectrolytes, hyaluronan and hylan, measured in the surface forces apparatus. *J. Biomed. Mater. Res. A*. 71:6–15.
10. Albersdorfer, A., and E. Sackmann. 1999. Swelling behavior and viscoelasticity ultrathin grafted hyaluronic acid films. *Eur. Phys. J. B*. 10:663–672.
11. Sengupta, K., J. Schilling, S. Marx, M. Fischer, A. Bacher, and E. Sackmann. 2003. Mimicking tissue surfaces by supported membrane coupled ultrathin layer of hyaluronic acid. *Langmuir*. 19:1775–1781.
12. Joester, D., E. Klein, B. Geiger, and L. Addadi. 2006. Temperature-sensitive micrometer-thick layers of hyaluronan grafted on microspheres. *J. Am. Chem. Soc*. 128:1119–1124.
13. Dubin-Thaler, B. J., G. Giannone, H. G. Dobereiner, and M. P. Sheetz. 2004. Nanometer analysis of cell spreading on matrix-coated surfaces reveals two distinct cell states and STEPs. *Biophys. J*. 86:1794–1806.
14. Nardi, J., T. Feder, R. Bruinsma, and E. Sackmann. 1997. Electrostatic adhesion between fluid membranes: phase separation and blistering. *Europhys. Lett*. 38:159–160.
15. Kloboucek, A., A. Behrisch, J. Faix, and E. Sackmann. 1999. Adhesion-induced receptor segregation and adhesion plaque formation: a model membrane study. *Biophys. J*. 77:2311–2328.
16. Cuvelier, D., and P. Nassoy. 2004. Hidden dynamics of vesicle adhesion induced by specific stickers. *Phys. Rev. Lett*. 93:228101.
17. Puech, P.-H., V. Askovic, P.-G. de Gennes, and F. Brochard-Wyart. 2006. Dynamics of vesicle adhesion: spreading versus dewetting coupled to binder diffusion. *Biophys. Rev. Lett*. 1:85–95.
18. Boulbitch, A., Z. Guttenberg, and E. Sackmann. 2001. Kinetics of membrane adhesion mediated by ligand-receptor interaction studied with a biomimetic system. *Biophys. J*. 81:2743–2751.
19. Limozin, L., A. Roth, and E. Sackmann. 2005. Microviscoelastic moduli of biomimetic cell envelopes. *Phys. Rev. Lett*. 95:178101–178104.
20. Kahya, N., D. Scherfeld, K. Bacia, and P. Schwille. 2004. Lipid domain formation and dynamics in giant unilamellar vesicles explored by fluorescence correlation spectroscopy. *J. Struct. Biol*. 147:77–89.
21. Sackmann, E., and R. F. Bruinsma. 2002. Cell adhesion as wetting transition? *ChemPhysChem*. 3:262–269.
22. Guttenberg, Z., B. Lorz, E. Sackmann, and A. Boulbitch. 2001. First-order transition between adhesion states in a system mimicking cell-tissue interaction. *Europhys. Lett*. 54:826–832.
23. Robert, P., L. Limozin, A. M. Benoliel, A. Pierres, and P. Bongrand. 2006. Glycocalyx regulation of cell adhesion. *In* Principles of Cellular Engineering: Understanding the Biomolecular Interface. M. R. King, editor. Elsevier Academic Press, Amsterdam, The Netherlands.
24. Radler, J., and E. Sackmann. 1993. Imaging optical thicknesses and separation distances of phospholipid- vesicles at solid surfaces. *J. Phys. II*. 3:727–748.
25. Wiegand, G., K. R. Neumaier, and E. Sackmann. 1998. Microinterferometry: three-dimensional reconstruction of surface microtopography for thin-film and wetting studies by reflection interference contrast microscopy (RICM). *Appl. Optics*. 37:6892–6905.
26. Schilling, J., K. Sengupta, S. Goennenwein, A. R. Bausch, and E. Sackmann. 2004. Absolute interfacial distance measurements by dual-wavelength reflection interference contrast microscopy. *Phys. Rev. E*. 69:021901.
27. Bereiter-Hahn, J., C. H. Fox, and B. Thorell. 1979. Quantitative reflection contrast microscopy of living cells. *J. Cell Biol*. 82: 768–779.
28. Schilling, J., E. Sackmann, and A. R. Bausch. 2004. Digital imaging processing for biophysical applications. *Rev. Sci. Instrum*. 75:2822–2827.
29. Jacob, M., T. Blu, and M. Unser. 2004. Efficient energies and algorithms for parametric snakes. *IEEE Trans. Immun. Proc*. 13:1231–1244.

30. Kuhl, T. L., J. Majewski, J. Y. Wong, S. Steinberg, D. E. Leckband, J. N. Israelachvili, and G. S. Smith. 1998. A neutron reflectivity study of polymer-modified phospholipid monolayers at the solid-solution interface: polyethylene glycol lipids on silane-modified substrates. *Biophys. J.* 75:2352–2362.

31. Sengupta, K., L. Limozin, M. Tristl, I. Haase, M. Fischer, and E. Sackmann. 2006. 2006. Coupling artificial actin cortices to biofunctionalized lipid monolayers. *Langmuir*. 22:5776–5785.

32. Ohya, T., and Y. Kaneko. 1970. Novel hyaluronidase from *Streptomyces*. *Biochim. Biophys. Acta*. 198:607–609.

33. Coelho-Neto, J., U. Agero, R. T. Gazzinelli, and O. N. Mesquita. 2006. Measuring optical and mechanical properties of a living cell with defocusing microscopy. *Biophys. J.* 91:1108–1115.

34. Selbi, W., A. J. Day, M. S. Rugg, C. Fulop, C. A. de la Motte, T. Bowen, V. C. Hascall, and A. O. Phillips. 2006. Overexpression of hyaluronan synthase 2 alters hyaluronan distribution and function in proximal tubular epithelial cells. *J. Am. Soc. Nephrol.* 17:1553–1567.

35. Henry, C. B., and B. R. Duling. 1999. Permeation of the luminal capillary glycocalyx is determined by hyaluronan. *Am. J. Physiol.* 277: H508–H514.

36. Tammi, R., D. MacCallumi, V. C. Hascall, J.-P. P. Ki, M. Hyttinen, and M. Tammi. 1998. Hyaluronan bound to CD44 on keratinocytes is displaced by hyaluronan decasaccharides and not hexasaccharides. *J. Biol. Chem.* 273:28878–28888.

37. Mummert, M. E., D. Mummert, D. Edelbaum, F. Hui, H. Matsue, and A. Takashima. 2002. Synthesis and surface expression of hyaluronan by dendritic cells and its potential role in antigen presentation. *J. Immunol.* 169:4322–4331.

38. Lee, G. M., B. Johnstone, K. Jacobson, and B. Caterson. 1993. The dynamic structure of the pericellular matrix on living cells. *J. Cell Biol.* 123:1899–1907.

39. Evanko, S. P., J. C. Angello, and T. N. Wight. 1999. Formation of hyaluronan- and versican-rich pericellular matrix is required for proliferation and migration of vascular smooth muscle cells. *Arterioscler. Thromb. Vasc. Biol.* 19:1004–1013.

40. Engler, A. J., S. Sen, H. L. Sweeney, and D. E. Discher. 2006. Matrix elasticity directs stem cell lineage specification. *Cell*. 126:677–689.

41. Ladam, G., L. Vonna, and E. Sackmann. 2005. Protrusion force transmission of amoeboid cells crawling on soft biological tissue. *Acta Biomater*. 1:485–497.

42. Marra, M., C. Cassinelli, A. Pavesion, and D. Reiner. 2003. Atomic force microscopy evaluation of aqueous interfaces of immobilized hyaluronan. *J. Colloids Interface Sci*. 259:236–243.

43. Bernard, A.-L., M. Guedeau-Boudeville, O. Sandre, S. Palacin, J.-M. di Meglio, and L. Jullien. 2000. Permeation through lipid bilayers by adhesion of giant vesicles on decorated surfaces. *Langmuir*. 16:6801–6808.

44. Bernard, A.-L., M.-A. Guedeau-Boudeville, L. Jullien, and J.-M. di Meglio. 2000. Strong adhesion of giant vesicles on surfaces: dynamics and permeability. *Langmuir*. 16:6809–6820.

45. Seveau, S., H. Keller, F. R. Maxfield, F. Piller, and L. Halbwachs-Mercarelli. 2000. Neutrophil polarity and locomotion are associated with surface redistribution of leukosialin (CD43), an antiadhesive membrane molecule. *Blood*. 95:2462–2470.

46. Sengupta, K., H. Aranda-Espinoza, L. A. Smith, P. A. Janmey, and D. A. Hammer. 2006. Spreading of neutrophils: from activation to migration. *Biophys. J.* 91:4638–4648.